Proceedings of the 4th WSEAS International Conference on Fluid Mechanics and Aerodynamics, Elounda, Greece, August 21-23, 2006 (pp168-173)

# Importance of the Navier-Stokes Forces on the Flow in a Hydrodynamic Torque Converter

MATTHIAS WOLLNIK, WERNER VOLGMANN, HORST STOFF
Fluid-Energy Machines
Ruhr-Universitaet
Universitaetsstr. 150, D-44780 Bochum
GERMANY

*Abstract:* The importance of the various influences acting on the flow field of a hydrodynamic torque converter is investigated in detail by analysing the individual terms of the time-averaged Navier-Stokes equations. Forces originating from pressure gradients, viscous and effective shear, Coriolis effect, convective and centrifugal acceleration are determined in several locations throughout the flow field. The velocity vector in magnitude and direction solved by a commercially available 3D computer code is the basis for the analysis. With increasing speed ratio of turbine-versus-pump the centrifugal force is dominant while shear forces become insignificant.

*Key–Words:* Hydrodynamic Torque Converter, Navier-Stokes Forces, Vane, Pump, Turbine

## 1 Introduction

The flow within hydrodynamic torque converters is highly complex. Although a lot of numerical and experimental efforts have been made to predict and analyse the flow in an automotive torque converter [1, 2, 3], it is still not fully understood how the operating behaviour can be tuned by shaping the geometry. Therefore an effort is made to understand how forces are acting on the fluid over a large range of operating conditions. Not only the absolute values of the individual Navier-Stokes terms but also the turning (yaw angle $\delta$) and the slope (pitch angle $\gamma$) of the flow field have to be analysed throughout the domain in order to get a comprehensive idea of the flow.

## 2 Problem Formulation

The forces acting within a hydrodynamic torque converter are analysed by solving the Navier-Stokes equation in the following steady-state formulation.

$$\overbrace{\rho \cdot (\vec{w} \cdot \nabla)\, \vec{w}}^{\text{convection force}} = \overbrace{-\nabla p}^{\text{pressure force}} \underbrace{+\rho \cdot \nu_{\text{eff}} \nabla^2 \vec{w}}_{\text{friction force}} \underbrace{-2\rho \cdot \vec{\omega} \times \vec{w}}_{\text{Coriolis force}} \underbrace{-\rho \cdot \vec{\omega} \times (\vec{\omega} \times \vec{r})}_{\text{centrifugal force}} \quad (1)$$

For a representative example a well-documented type of hydrodynamic torque converter is chosen to show how the individual forces act on the fluid flow revolving in a toroidal domain. In the past the Navier-Stokes equation had been solved for the whole domain without investigating the importance of the individual contributions.

## 3 Problem Solution

### 3.1 Torque converter CFD model

The torque converter used in this study is the model W240 by Fichtel & Sachs with the channel contour shown in figure 1. It is documented in the book of Förster [4], its cross section is nearly spherical and has a nominal outer diameter of $D = 240$ mm. It contains 11 stator vanes, 31 blades in the impeller of the pump and 29 blades in the turbine. One blade passage is modelled for each component. Clearances between blades and shell as well as core are neglected and the pump domain was circumferentially positioned so that the exit of the pump blade points to the middle of a turbine blade passage. Each component has its own

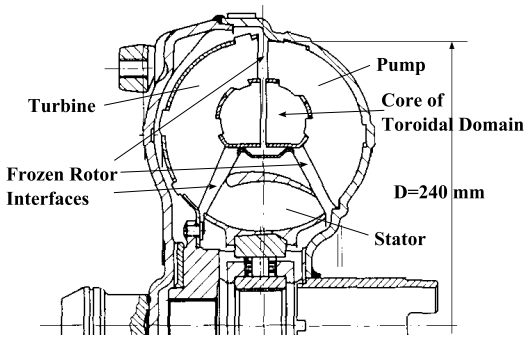


**Fig. 1:** Section of a toroidal bladed channel [4].

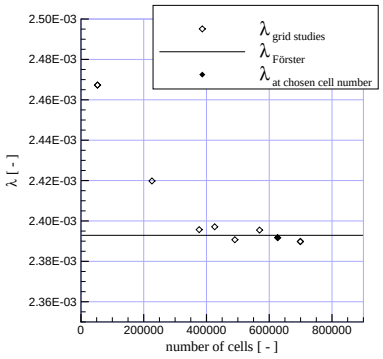


**Fig. 2:** Grid refinement studies showing $\lambda = \frac{M_P}{\rho\omega^2 D^5}$, the pump torque coefficient, versus the number of cells at $SR = 0.01$.

frame of reference in order to analyse the characteristic operating lines with the speed ratio of turbine-versus-pump of $SR = 0.01$, 0.4 and 0.8 at a pump speed of 2000 $\mathrm{min}^{-1}$. Therefore the complete characteristics were interpolated corresponding to these results.

At the interfaces between the components a frozen rotor model is used. A steady-state flow field is assumed as well as circumferential periodicity for each of the components. Physical properties as for example density $\rho$, kinematic viscosity $\nu$ and temperatures are assumed to remain constant for simulating the flow with the commercial flow solver CFX10.1. The calculated effective kinematic viscosity $\nu_{\mathrm{eff}}$ in equation 1 is due to effective shear and therefore contains molecular and turbulent viscosity. Also the CFX - "Specify Blend Factor" is set to a value of 1.0 so that the flow is solved with Second Order differencing for the advection terms.

Preliminary investigations concerning the size of the grid showed, that a grid with a total of about 620 000 cells provides appropriate grid-independent numerical solutions. The development of the computational solution with increasing numbers of cells are displayed in figure 2. Figure 3 gives a detailed view of the stator grid near the hub.

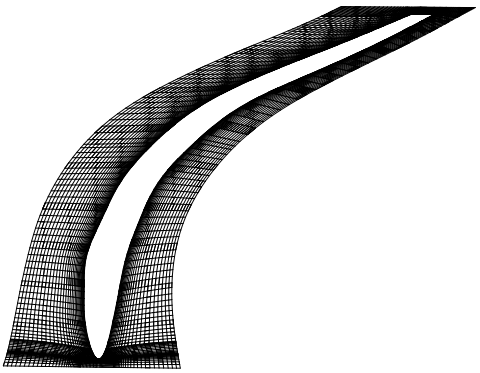

**Fig. 3:** Computational grid at hub of stator.

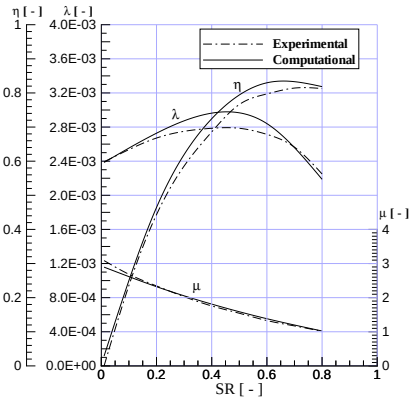


**Fig. 4:** Operating performance of type W240 for pump torque coefficient $\lambda$, torque conversion $\mu$ and efficiency $\eta$.

As shown in figure 4 the computational torque converter characteristics compare very well to the experimental results, considering the lack of information concerning the density, viscosity and temperature of the oil used during the measurements. The average discrepancy is less than 3.3% for the power number $\frac{\Delta\lambda}{\lambda}$ and less than 3.1% for the torque conversion number $\frac{\Delta\mu}{\mu}$ and the efficiency $\frac{\Delta\eta}{\eta}$, respectively.

## 3.2 Angle definitions

For describing a vector $\vec{X}$ in a three-dimensional domain it is necessary to have its modulus $|\vec{X}|$ and the direction of this vector expressed through the flow turning (pitch angle $\gamma$) and the slope (yaw angle $\delta$). These angles are used in the commonly employed NACA-definition parting from the centerline of the shaft like in bladings of the axial turbomachinery. Due to the fact that the machine axis is used as a reference, problems occur in radial machines. Especially in the pump and the turbine of automotive torque converters, where the principal flow direction changes by 360°, the standard NACA-definition fails.

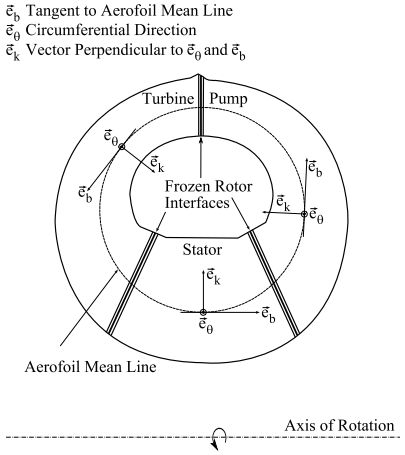


**Fig. 5:** Meridional section

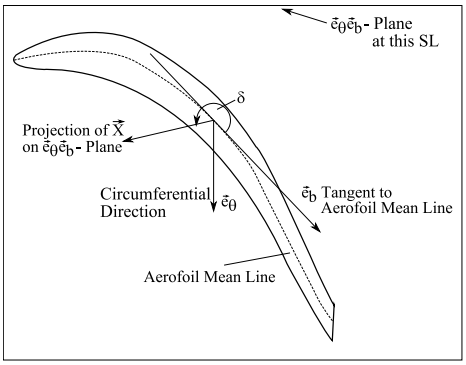


**Fig. 6:** Definition of yaw angle $\delta$.

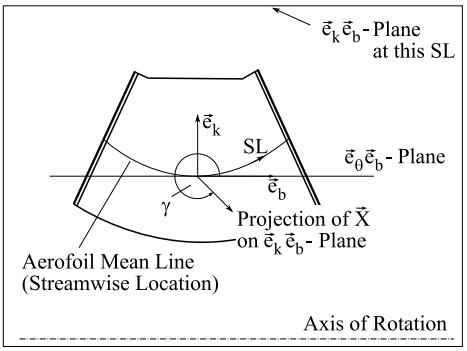


**Fig. 7:** Definition of pitch angle $\gamma$.

Therefore the flow direction, prescribed by the aerofoil, is represented by one polygon line at half-span and pointing in streamwise direction (figure 5). This flow direction is used as the reference for the upcoming angle definitions.

At each constant streamwise location ($SL$) a quasi-tangential plane $\vec{e}_\theta\vec{e}_b$ is created between the circumferential direction $\vec{e}_\theta$ and the tangent to the aerofoil mean line $\vec{e}_b$. In this plane the flow turning (yaw angle $\delta$) between the vector $\vec{X}$, representing the individual Navier-Stokes-Forces or the mean velocity, and the tangent to the aerofoil mean line $\vec{e}_b$ is measured. Therefore the yaw angle $\delta$ can be calculated using the projection $\vec{X}_{\vec{e}_\theta\vec{e}_b}$ of vector $\vec{X}$ onto the $\vec{e}_\theta\vec{e}_b$-plane:

$$\delta = \operatorname{acos}\frac{\vec{e}_b\cdot\vec{X}_{\vec{e}_\theta\vec{e}_b}}{|\vec{e}_b|\cdot|\vec{X}_{\vec{e}_\theta\vec{e}_b}|} \quad (2)$$

$$= \operatorname{acos}\frac{\vec{e}_b\cdot\left(\vec{X}-\vec{X}_{\vec{e}_k}\right)}{|\vec{e}_b|\cdot|\left(\vec{X}-\vec{X}_{\vec{e}_k}\right)|}. \quad (3)$$

An exemplary configuration for the stator as well as the above mentioned polygon line can be seen in figure 6.

According to figure 7 the slope (pitch angle $\gamma$) is created between the vector $\vec{e}_b$ and the projection $\vec{X}_{\vec{e}_k\vec{e}_b}$ of vector $\vec{X}$ onto the quasi-tangential plane $\vec{e}_k\vec{e}_b$. The pitch angle $\gamma$ is therefore defined by:

$$\gamma = \operatorname{acos}\frac{\vec{e}_b\cdot\vec{X}_{\vec{e}_k\vec{e}_b}}{|\vec{e}_b|\cdot|\vec{X}_{\vec{e}_k\vec{e}_b}|} \quad (4)$$

$$= \operatorname{acos}\frac{\vec{e}_b\cdot\left(\vec{X}_{\vec{e}_k}+\vec{X}_{\vec{e}_b}\right)}{|\vec{e}_b|\cdot|\left(\vec{X}_{\vec{e}_k}+\vec{X}_{\vec{e}_b}\right)|}. \quad (5)$$

The vector $\vec{e}_k = \vec{e}_\theta \times \vec{e}_b$ is perpendicular to the circumferential direction $\vec{e}_\theta$ and the aerofoil direction $\vec{e}_b$ and points to the core of the torque converter's computational domain (figure 5).

The combination of both angle definitions yields to a three-dimensional figure (figure 8), which shows both the directions ($\vec{e}_\theta$, $\vec{e}_b$ and $\vec{e}_k$) and the projections onto the planes ($\vec{X}_{\vec{e}_k\vec{e}_b}$ and $\vec{X}_{\vec{e}_\theta\vec{e}_b}$). The angles $\delta$ and $\gamma$ in this right-hand system $\vec{e}_\theta$, $\vec{e}_b$ and $\vec{e}_k$ are defined starting from the reference plains $\vec{X}_{\vec{e}_k\vec{e}_b}$ and $\vec{X}_{\vec{e}_\theta\vec{e}_b}$, respectively. A vector $\vec{X}$, identical with the blade surface direction $\vec{e}_b$, refers to the values of $\delta = 0°$ and $\gamma = 0°$.

Additionally, figure 8 contains the projection of $\vec{X}$ on the meridional plane, necessary for a modified definition of $\beta_{\text{NACA}}$ with the meridional flow direction instead of the machine axis as the reference. The definition used at the Ruhr-Universitaet is the peripheral flow turning $\beta$ defined as the counter-clockwise angle between the circumferential direction $\vec{e}_\theta$ and the tangent to the aerofoil mean line $\vec{e}_b$.

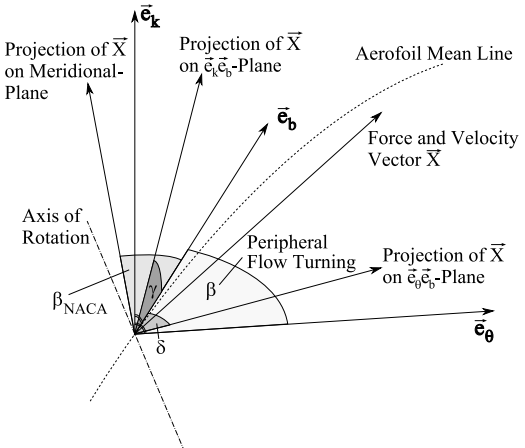


**Fig. 8:** Yaw angle $\delta$ and pitch angle $\gamma$ for deflection and slope of the toroidal flow.

Contrary to this chosen approach of decomposing the Navier-Stokes equation throughout the entire torque converter Marathe and Lakshminarayana analysed the pitch and yaw angles in a turbine and a stator [5] and in a pump [6] by using the NACA angle convention. However their analysis is limited to the inlet and exit planes of these components, of which the surface vectors are almost parallel to the axis of rotation. There-

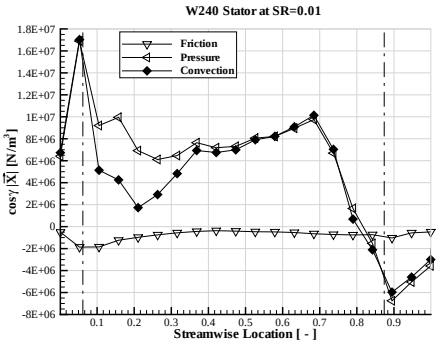


**Fig. 9:** Streamwise forces by Navier-Stokes terms in stator.

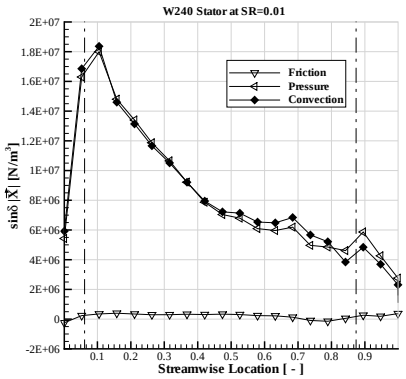


**Fig. 10:** Peripheral forces by Navier-Stokes terms in stator.

fore the NACA angle convention was convenient.

### 3.3 Navier-Stokes term averaging

In order to follow the forces by Navier-Stokes terms and the mean velocity along the streamwise direction through the entire torque converter, these forces are averaged for each location along this stream path. Thus the x-, y- and z-components are momentum-averaged on cross sections at constant streamwise locations.

As a result averaged vectors $\vec{X}$ for every Navier-Stokes term and the mean velocity, respectively, are calculated at a certain streamwise location. The vector $\vec{X}$ is used to examine the pitch angle and the yaw angle of each term in the Navier-Stokes equation throughout the domain applying equation 2 and equation 4, respectively.

### 3.4 Scaled absolute contributing terms

As mentioned earlier it is necessary to know the length of a vector in addition to the pitch and the yaw angle. In order to combine the information about size and direction, the absolute values of the individual Navier-Stokes terms are scaled. The factor $\cos\gamma$ is used for the contribution to accelerate/decelerate the flow in streamwise direction while the factor $\sin\delta$ is used for the contribution to the peripheral momentum transmission. For analysing the influence on the absolute mean velocity, the $\cos\gamma$-scaled forces are accumulated. Due to the fact that three different domains are analysed, the Navier-Stokes equation (1) has to be solved independently for the individual torque converter components.

The graphical display in each following figure contains vertical dash-dotted lines, indicating the leading edges and trailing edges of blades and vanes. Although the angle distribution through the entire torque converter was analysed for the $0.01, 0.4$ and $0.8$ speed ratios, only the results for $SR = 0.01$ are shown.

#### 3.4.1 Stator

As the stator domain is stationary, only the forces due to convection, pressure and friction appear in figure 9 to figure 11. Additionally the absolute mean velocity values are shown in the last-mentioned figure. The scaling of the friction force, which points almost in opposite direction of the mean-line vector $\vec{e}_b$, emphasizes the influence in the $\cos\gamma$-scaled figure 9 and lowers the influence in the $\sin\delta$-scaled figure 10. For the speed ratio of $SR = 0.01$ the absolute value of the scaled friction force is therefore about one order of magnitude smaller than the scaled absolute values of the convection force and the pressure force, which are dominating the flow at this speed ratio. These forces are acting in flow direction up to a region in front of the trailing edge, where a change in signs shows a turn back in the acting direction (figure 9).

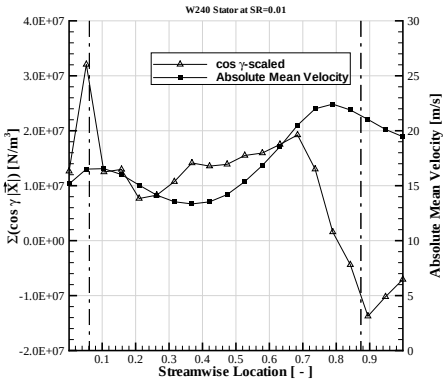


**Fig. 11:** Accumulated streamwise forces by Navier-Stokes terms in stator.

The $\sin\delta$-scaled forces in figure 10 indicate the distribution of the torque converting forces within the stator. Due to the large incidence angles the peaks for the scaled friction and pressure forces are near the leading edge. The well channeled flow further down the stream explains the decrease in $\sin\delta$-scaled forces.

In figure 11 the accumulated $\cos\gamma$-scaled forces are shown with the absolute mean velocity in the stator. The influence of the forces in streamwise direction on the acceleration/deceleration of the absolute mean velocity takes effect with a short delay.

### 3.4.2 Turbine

In addition to the forces already described in the previous subsection, the Coriolis force and the centrifugal force occur due to the rotating frame of reference. At the speed ratio $SR = 0.01$ these additional forces, like the shear force, play only a minor role, though. Therefore the flow in the turbine is dominated by the pressure force and the convection force.

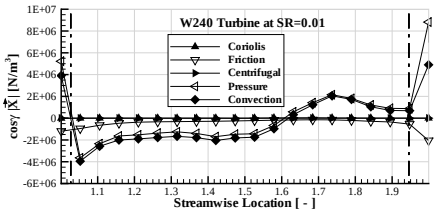


**Fig. 12:** Streamwise forces by Navier-Stokes terms in turbine.

As well as in the stator, the shear force vector points in opposite directions of the blade-metal vector $\vec{e}_b$ in almost the whole turbine, therefore emphasizing the $\cos\gamma$-scaled values (figure 12) and lowering the $\sin\delta$-scaled contributions (figure 13). Nevertheless, at this speed ratio of $SR = 0.01$ the shear force is about one order of magnitude smaller than the dominating scaled pressure and convection forces. As shown in figure 12 the scaled pressure and convection forces are acting opposite to the tangent direction of the aerofoil mean line between the leading edge and 60% of the turbine's streamwise location ($1.03 \leq SL \leq 1.61$). Opposed to this these force act in streamwise direction in the other parts of the turbine domain. The large positive values for the scaled pressure and convection forces indicate an large incidence angle in front of the leading edge. This high incidence angle is also responsible for high negative values of the $\sin\delta$-scaled pressure and convection forces near the inlet in figure 13. Due to the slowly turning turbine the incidence angles are high at the exit of the domain, causing jumps in the lines. Between the edges of the turbine the trends for the dominant forces run almost parallel, reaching their minimum in the middle of the domain.

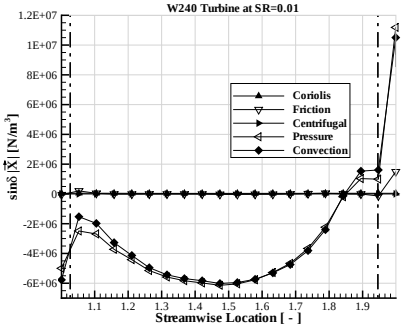


**Fig. 13:** Peripheral forces by Navier-Stokes terms in turbine.

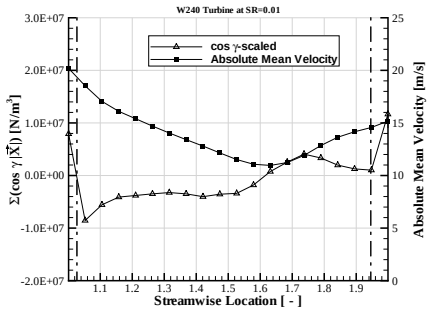


**Fig. 14:** Accumulated streamwise forces by Navier-Stokes terms in Turbine.

Like in the stator, the absolute mean velocity follows the accumulated force's trend. Negative force values slow down the flow until $SL = 1.61$ in the turbine domain. The flow accelerates again with positive scaled forces to the end of the domain.

### 3.4.3 Pump

Contrary to the turbine at the speed ratio of $SR = 0.01$, the rotational velocity of $2000\ \mathrm{min}^{-1}$ generates Coriolis and centrifugal forces which are no more negligible.

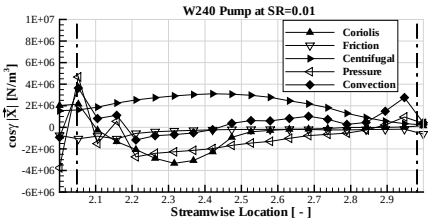


**Fig. 15:** Streamwise forces by Navier-Stokes terms in pump.

Like in the other two domains the friction force is pointed against the blade-metal vector $\vec{e}_b$ and the absolute value is smaller than the values of the other forces. Due to the large incidence angles at the leading edge of the pump, positive $\cos\gamma$-scaled values appear (figure 15). After 10% of the domain the flow is well channeled with centrifugal force values that accelerate the flow. While the $\cos\gamma$-scaled centrifugal force stays positive, changes in signs occur for the other $\cos\gamma$-scaled forces. Up to $SL = 2.2$ and after $SL = 2.42$ the pressure force contributes to the acceleration of the flow. Inbetween these $SL$ the scaled pressure force decelerates the flow. Due to the averaging on surfaces at constant streamwise locations, the Coriolis force has a component pointing against the tangent to the aerofoil mean line $\vec{e}_b$. This component reaches its maximum absolute value at about 35% of the pump domain. The scaled convection force is again parallel to the scaled pressure force though the distance is larger than in the other domains at the $SR = 0.01$. Like in the other domains at this speed ratio, the $\sin\delta$-scaled

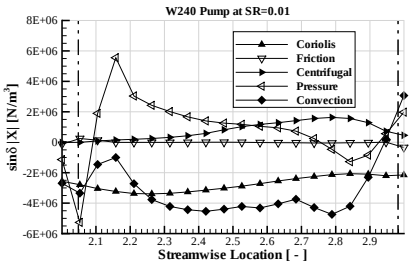


**Fig. 16:** Peripheral forces by Navier-Stokes terms in pump.

shear force has the lowest influence on the torque conversion. Although the $\cos\gamma$-scaled centrifugal force is a main contributor in figure 15, the $\sin\delta$-scaled centrifugal force play only a minor role in figure 16. The $\sin\delta$-scaled Coriolis force, which is almost constant over the entire pump domain, is one of the dominant $\sin\delta$-scaled forces. Together with the pressure force, these two $\sin\delta$-scaled forces act the same direction, while the $\sin\delta$-scaled convection force acts in the opposite direction between $SL = 2.1$ and $SL = 2.75$.

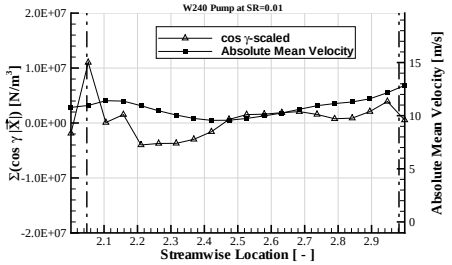


**Fig. 17:** Accumulated streamwise forces by Navier-Stokes terms in pump.

The trend that the absolute mean velocity follows the accumulated $\cos\gamma$-scaled forces is confirmed for the pump (figure 17). Only in the regions with negative sums for the $\cos\gamma$-scaled forces, the flow is decelerated.

# 4 Conclusion

The steady-state distribution of forces due to the five Navier-Stokes terms has been determined. These forces are described in detail for the absolute values scaled with $\cos\gamma$ (streamwise) and $\sin\delta$ (peripheral), respectively. With an increasing rotational velocity the centrifugal force becomes dominant in pump and turbine. Contrary to the centrifugally accelerated flow in the pump the flow is decelerated through the centrifugal force in the turbine. The shear force is decreasing with increasing speed ratios due to lower velocities and mass flow rates. Therefore the influence on the averaged velocity along the streamwise direction is limited. In this investigation the Coriolis force has components in streamwise direction because of the averaging on surfaces at constant streamwise locations. The pressure force and the convection force have almost the same characteristic lines for the stator. The difference is caused by the friction force. In the turbine the pressure force and convection force lines tend to separate the more the speed ratio rises. The reason for this is the growing influence of the forces depending on the rotational velocity while the friction force stays at a low level. Though the pump is rotating at a constant $2000\ \mathrm{min}^{-1}$, an influence of the speed ratio is noticeable by changing incidence angles and varying mass flow rates. The pressure force as well as the convection force show the influence of the large incidence angles behind the leading edge by jumps in the corresponding distributions.

# 5 Acknowledgments

The authors would like to express their acknowledgement to Deutsche Forschungsgemeinschaft (DFG) for the financial support of the project.

*References:*

[1] Ackermann J.: *Experimentelle und numerische Strömungsuntersuchung eines Trilok-Drehmomentwandlers mit schmaler Kreislaufform*, Vol. 421 of *Reihe 7 Strömungstechnik*. VDI Verlag, Düsseldorf, 1st edn., 2001.

[2] Habsieger A., Flack R.: Flow Characteristics at the Pump-Turbine Interface of a Torque Converter at Extreme Speed Ratios. *International Journal of Rotating Turbomachinery*, Vol. 9, 2003, pp. 419–426.

[3] Schweitzer J., Gandham J.: Computational Fluid Dynamics in Torque Converters: Validation and Application. *International Journal of Rotating Turbomachinery*, Vol. 9, 2003, pp. 411–418.

[4] Förster H.J.: *Automatische Fahrzeuggetriebe : Grundlagen, Bauformen, Eigenschaften, Besonderheiten*. Springer-Verlag, Berlin et al., 1990.

[5] Marathe B.V., Lakshminarayana B.: Experimental Investigation of Steady and Unsteady Flow Field Downstream of an Automotive Torque Converter Turbine and Stator. *International Journal of Rotating Turbomachinery*, Vol. 2, No. 2, 1995, pp. 67–84.

[6] Marathe B.V., Lakshminarayana B.: Experimental Investigation of Steady and Unsteady Flow Field Downstream of an Automotive Torque Converter Pump. *International Journal of Rotating Turbomachinery*, Vol. 5, No. 2, 1999, pp. 99–116.